Why $Pb(B_{1/3}B'_{2/3})O_3$ Perovskites Disorder More Easily than $Ba(B_{1/3}B'_{2/3})O_3$ Perovskites and the Thermodynamics of 1:1-type Short Range Order in PMN

B.P. Burton [a]

[a] *Materials Science and Engineering Laboratory, Ceramics Division*
National Institute of Standards and Technology, Gaithersburg, MD 20899

Published in J. Phys. Chem. Solids **61**, 327- (2000)

Abstract

Fully relaxed, planewave pseudopotential calculations of formation energies (ΔE) were performed for ordered supercells in the perovskite based system $(1-X)\cdot PbNbO_3 - (X)\cdot PbMgO_3$, including six different supercells at the $X = 1/3$ composition $[Pb(Mg_{1/3}Nb_{2/3})O_3;\ PMN]$. Some of the corresponding supercell calculations were also performed for the eight different stoichiometries of $A(B_{1/3}B'_{2/3})O_3$ perovskite in which $A = Pb,\ Ba$ and $B = Zn,\ Mg$ and $B' = Nb,\ Ta$. A striking difference between the $Pb(B_{1/3}B'_{2/3})O_3$ systems and the $Ba(B_{1/3}B'_{2/3})O_3$ systems is that the differences in formation energies for any $Pb(B_{1/3}B'_{2/3})O_3$ system are roughly an order of magnitude smaller than those for the corresponding $Ba(B_{1/3}B'_{2/3})O_3$ system, which indicates that the energetic barriers to disordering are much lower in the $Pb(B_{1/3}B'_{2/3})O_3$ systems. The range of energies spanned by various PMN-stoichiometry supercells is particularly narrow, suggesting that cation disorder should persist to lower temperatures in PMN than in any of the others. Ising type thermodynamic models, that are roughly consistent with the ΔE results, were used to simulate the finite temperature behavior of a prototype $A(B_{1/3}B'_{2/3})O_3$ perovskite that exhibits the transition sequence $1:2 \rightarrow 1:1 \rightarrow$ *Disordered*. This model reproduces the characteristic microstructure of PMN, and explains it in terms of *equilibrium* $1:1$ short range order in the disordered phase.

Key words: PMN; First Principles; Phase Diagram; Order-Disorder; $A(B_{1/3}B'_{2/3})O_3$ perovskites

1 Introduction

The structure of PMN is controversial. Based on high resolution electron microscopy Krause et. al.(1) described it as a disordered perovskite with $2-5nm$ ordered microdomains that generate diffuse $(h/2, k/2, l/2)$ h, k, l *odd* reflections(2). Small angle resonant x-ray scattering studies(3) indicate that *locally* PMN adopts a NaCl-type 1:1 $Fm\overline{3}m$ ($a_{1:1} \sim 2a_0$) structure in which one $B-site$ is occupied by Nb ions while the other has approximately 1/3 Nb plus 2/3 Mg. This is sometimes referred to as the *random site model*, and a similar structure is reported for $Zr-doped$ PZN(4). Recently, Davies (5) has shown that $1:1$ long-range order (LRO) is observed in $Pb(Mg_{1/3}Ta_{2/3})O_3$ at temperatures $T \leq 1350C$ after $12hrs$ annealing. This latter result is particularly significant, because the substitution of Ta for Nb in an $A(B_{1/3}B'_{2/3})O_3$ perovskite typically increases the transition temperature for an order-disorder transition. For example, $Ba(Zn_{1/3}Nb_{2/3})O_3$ disorders, $1:2 \rightarrow DIS$, at $\sim 1375C$(6), whereas $Ba(Zn_{1/3}Ta_{2/3})O_3$ remains in the ordered $1:2$ structure up to at least $1650°C$ (7; 8). It follows that one might expect a $1:1$ phase to be stable in PMN, but to disorder at a lower temperature than the corresponding phase in PMT.

A space-charge model has also been proposed for PMN (9; 2; 11; 10; 12). It postulates that small regions with $1:1$ order, and approximately $1:1$ $Mg:Nb$ composition, modulate coherently with disordered regions that are sufficiently Nb-enriched to maintain global charge balance. The failure of PMN ordered microdomains to coarsen, after $30hrs$ *at* $900°C$, was cited as evidence in favor of the space-charge model (2; 11); the idea being that the creation of compositional fluctuations, which imply charge fluctuations, creates an energetic barrier to coarsening. Both structural models imply significant configurational entropy which precludes either as a GS. Therefore, it seems unavoidable that the observed state of PMN is metastable, and fails to reach its true GS because of unfavorable kinetics.

2 Total Energy Calculations

Formation energies [ΔE relative to $(1-X)\cdot PbNbO_3-(X)\cdot PbMgO_3$] were calculated for a number of ordered structures (Table 1; Figures 1 and 2) using the Vienna *ab initio* simulation program (VASP)(13). These are plane-wave pseudopotential calculations that are performed in the local density approximation for exchange and correlation energies. Electronic degrees of freedom were optimized with a conjugate gradient algorithm, and both cell constant and ionic positions were fully relaxed. Valence electron configurations for the various

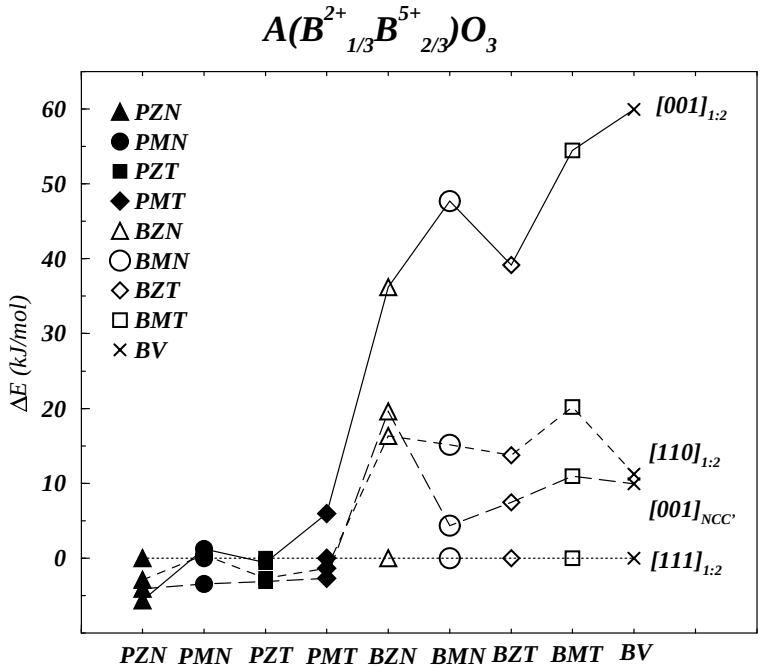

Fig. 1. Comparison of formation energies, $\Delta E's$, for various perovskite based supercells with compositions $A(B_{1/3}B'_{2/3})O_3$; $A = Pb,\ Ba\ \ B = Mg,\ Zn\ \ B' = Nb,\ Ta$. **Note that results for the $[001]_{NCC'}$ structure do NOT appear in the published article**

pseudopotentials are: $Pb\ 6s^2 5d^{10} 6p^2$ (Pb_d version); $Mg\ 2p^6 3s^2$ ($\mathrm{Mv}_p v$ version); $Nb\ 4p^6 5s 4d^4$; O $2p^6$, and an energy cutoff of 395.7 eV was used. All calculations were performed with the "high precision" option which guarantees that *absolute* energies are converged to within a few meV. To promote cancellation of errors, formation energies for the $PbNbO_3$ and $PbMgO_3$ reference states, are calculated for each supercell with identical K-point meshes.

Superstructures and VASP results for $\Delta E's$ and cell volumes are reported in Table 1. Most structure names are in the form $[hkl]_{N,M,..}$ where the subscript $NM...$ specifies a sequence of $B-site$ cation layers perpendicular to the vector $[hkl]_{cubic}$. For example the 1:2 phase, which is the BZT GS, is represented as $[111]_{NNM}$ indicating a $...(Nb)-(Nb)-(Mg)...$ layer sequence perpendicular to [111]; similarly, $[111]_{NMM}$ indicates a $...(Nb)-(Mg)-(Mg)...$ layer sequence perpendicular to [111]. Subscripts T and C indicate triangular and chessboard layers respectively (Figure 3). As shown in Figure 4a, the $[001]_{NCC'}$ structure has adjacent chessboard layers between which all nearest neighbor (nn) $B-B$ pairs are in configuration $Nb-Mg$; whereas the corresponding nn pairs in the $[001]_{NCC}$ structure (Figure 4b) are in configurations $Nb-Nb$ or $Mg-Mg$.

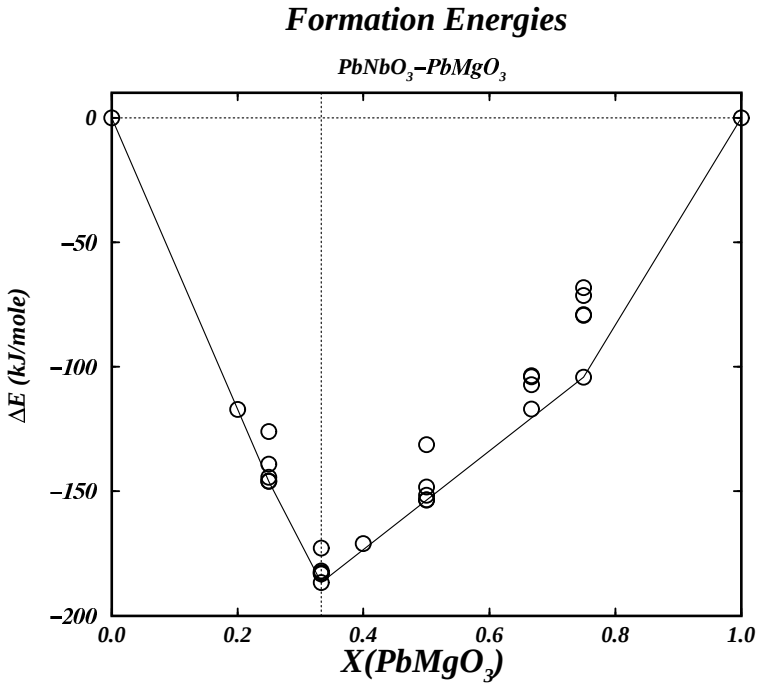

Fig. 2. Formation energies, $\Delta E's$, for various perovskite based supercells in the system $(1-X)\cdot PbNbO_3-(X)\cdot PbMgO_3$.

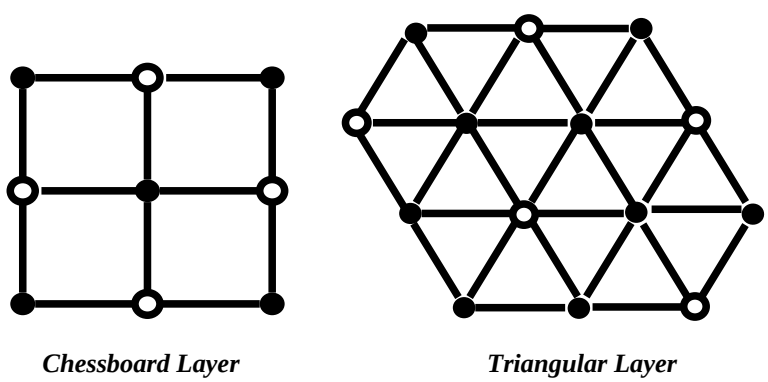

Fig. 3. Layer motifs referred to in Table 1: $\bullet = Nb$, $\circ = Mg$.

(1) *For the cell that was used in the VASP calculation which often is not the wholosymmetric cell listed in column* 2. *For example, calculations for the BCC structure phases at* $X = 1/4$ *and*
$X = 3/4$ *were done on a cell with domensions* $\sqrt{3}\ \ \sqrt{3}\ \ \sqrt{3}$.
(2) *One mol* $= ABO_3$. (3) *Ideal Perovskite.* (4) *Candidate PMN GS.*
(5) $1:2$ *structure.* (6) *3tri structure*[13]. (7) $NaCl-$*type structure.*

Table 1
VASP results for $(1-X)\cdot PbNbO_3-(X)\cdot PbMgO_3$ supercells.

System	*Space Group*	*Cell* (a_{cubic}) a b c	$k-mesh^{(1)}$	X	V $au^3/mol^{(2)}$	ΔE kJ/mol	ΔV au^3/mol
$PbNbO_3$ (3)	$P\overline{3}m1$	1 1 1	8 8 8	0	431.92	0	0
$\sqrt{5}x\sqrt{5}x1$	$P4/mmm$	$\sqrt{5}$ $\sqrt{5}$ 1	4 4 9	1/5	438.86	-121.21	-6.95
$[001]_{NNNNM}$	$P4/mmm$	1 1 5	10 10 2	1/5	441.15	-117.23	6.98
$[001]_{NNNM}$	$P4/mmm$	1 1 4	8 8 2	1/4	431.08	-146.10	-0.74
$2x2x1$	$P4/mmm$	2 2 1	4 4 8	1/4	435.60	-145.91	3.67
$[110]_{NNNM}$	$Pmmm$	$2\sqrt{2}$ $\sqrt{2}$ 1	8 4 12	1/4	438.42	-144.40	6.77
$[001]_{NC}$	$P4/mmm$	$\sqrt{2}$ $\sqrt{2}$ 2	8 8 4	1/4	435.61	-138.48	6.51
BCC	$Im\overline{3}m$	2 2 2	6 6 6	1/4	437.03	-125.03	5.52
$[001]_{NCC'}$ (4)	$P4/nmm$	$\sqrt{2}$ $\sqrt{2}$ 3	7 7 3	1/3	431.67	-185.85	5.22
$[111]_{NNM}$ (5)	$P\overline{3}m1$	$\sqrt{2}$ $\sqrt{2}$ $\sqrt{3}$	5 5 4	1/3	431.38	-183.22	4.17
$[110]_{NNM}$ (6)	$Amm2$	$3\sqrt{2}$ $\sqrt{2}$ 1	4 4 10	1/3	436.25	-182.81	9.30
$[001]_{NNM}$	$P4/mmm$	1 1 3	6 6 2	1/3	436.76	-182.03	10.11
$[111]_{NT}$	$Immm^*$	$\sqrt{2}$ $\sqrt{2}$ 4	2 6 3	1/3	455.80	-177.92	29.13
$[001]_{NCC}$	$P/4mmm$	$\sqrt{2}$ $\sqrt{2}$ 3	7 7 3	1/3	434.25	-172.81	16.55
$[001]_{NNMM}$	$P4/mmm$	1 1 4	8 8 2	1/2	431.59	-153.59	14.00
$[110]_{NNMM}$	$Pmm2$	$2\sqrt{2}$ $\sqrt{2}$ 1	8 4 12	1/2	430.11	-153.47	12.69
$[001]_{NM}$	$P4/mmm$	1 1 2	8 8 4	1/2	425.44	-151.59	7.68
$[111]_{NM}$ (7)	$Fm\overline{3}m$	2 2 2	4 4 4	1/2	424.22	-148.25	6.38
$[110]_{NM}$	$P4/mmm$	$\sqrt{2}$ $\sqrt{2}$ 1	7 7 10	1/2	425.40	-131.27	7.65
$[001]_{NMM}$	$P4/mmm$	1 1 3	6 6 2	2/3	421.41	-116.92	13.64
$[111]_{NMM}$	$P\overline{3}m1$	$\sqrt{2}$ $\sqrt{2}$ $\sqrt{3}$	5 5 4	2/3	421.03	-107.24	12.21
$[110]_{NMM}$	$Amm2$	$3\sqrt{2}$ $\sqrt{2}$ 1	4 4 10	2/3	420.46	-103.51	12.16
$[001]_{NMMM}$	$P4/mmm$	1 1 4	8 8 2	3/4	425.35	-104.21	21.99
$[001]_{NC}$	$P4/mmm$	$\sqrt{2}$ $\sqrt{2}$ 2	8 8 4	3/4	410.53	-79.07	14.84
$2x2x1$	$P4/mmm$	2 2 1	4 4 8	3/4	410.51	-77.65	6.77
$[110]_{NMMM}$	$Pmmm$	$2\sqrt{2}$ $\sqrt{2}$ 1	8 4 12	3/4	402.46	-77.38	-1.07
BCC	$Im\overline{3}m$	2 2 2	6 6 6	3/4	409.97	-66.45	6.84
$[001]_{MMMMN}$	$P4/mmm$	1 1 5	10 10 2	4/5	427.03	-97.91	26.62
$PbMgO_3$ (3)	$P\overline{3}m1$	1 1 1	8 8 8	1	389.04	0	0

Figure 1 shows results for the $[111]_{NNM}$, $[110]_{NNM}$ and $[001]_{NNM}$ superstructures for the eight possible stoichiometries in which $A = Pb,\ Ba$, $B = Zn,\ Mg$ and $B' = Nb,\ Ta$; $\Delta E([111]_{NNM}) \equiv 0$. Lines connect $\Delta E's$ for the same superstructure with different stoichiometries. Four aspects of Figure 1, and Table 1, stand out:

- Substituting Pb for Ba on the $A-site$ significantly reduces the differences between various $\Delta E's$.
- All Ba-perovskites exhibit the same formation energy hierarchy: $\Delta E([111]_{NNM}) < \Delta E([110]_{NNM}) < \Delta E([001]_{NNM})$, but the $Pb(B_{1/3}, B'_{2/3})O_3$ systems do not.
- $\Delta E([001]_{NCC'})$ is lowest at the PMN stoichiometry (Table 1), which makes the $[001]_{NCC'}$ structure a candidate GS.
- The PMN results span a much smaller energy range than any other stoichiometry, which implies that PMN should disorder at a lower temperature than any of the others.

It is reasonable to argue that the configurational excess energy is dominated by two contributions: long-range Coulomb interactions which favor configurations that maximize unlike charges on nn $B - sites$; and short-range interactions that are primarily associated with the optimization of $A - O$ bonds. Long-range electrostatic interactions dominate when the $A - cation$ is the larger more regularly coordinated Ba^{2+}, and short-range interactions become competitive when the $A - cation$ is the smaller less regularly coordinated Pb^{2+}. Bellaiche and Vanderbilt(14) showed that an electrostatic model of $B - site$ ordering in $A(B_{1/3}, B'_{2/3})O_3$ perovskites (a 1:2 mixture of screened 2^- and 1^+ point charges on a simple cubic 6x6x6 supercell) predicts a $1:2$ GS and a $1:2 \rightarrow DIS$ transition sequence. This is consistent with the ΔE hierarchies calculated for $Ba(B_{1/3}, B'_{2/3})O_3$ systems, but not with those for the $Pb(B_{1/3}, B'_{2/3})O_3$ systems. For example, the concentrations of electrostatically unfavorable $Mg - O - Mg$ triplets increases monotonically (0, 1/9, 2/9) in the sequence of structures $[111]_{NNM}$, $[110]_{NNM}$, and $[001]_{NNM}$ respectively, and as expected $\Delta E's$ for the $Ba-$systems increase monotonically as well. In the $Pb-$systems however, this correlation does not hold. Substitution of Pb for Ba on the $A - site$ drastically reduces the differences in energy between various $B - site$ configurations, which implies that energetically favorable $Pb - O$ relaxations *anticorrelate* with electrostatically favorable $B - site$ configurations. That is, as the concentration of electrostatically unfavorable configurations in a $Pb(B_{1/3}, B'_{2/3})O_3$ perovskite increases, the concentration of stabilizing $Pb - O$ bonds also increases leading to a very small change in configurational energy.

The most plausible explanation for these results is that hybridization of O $2p$ states and Pb $6s$ lone-pair states(14; 15; 16; 17; 18) stabilize electrostat-

ically unfavorable configurations; specifically via short $Pb-O$ bonds to the otherwise underbonded oxygens in $B^{2+}-O-B^{2+}$ triplets. Disordering creates $B^{2+}-O-B^{2+}$ triplets with underbonded oxygens, and increases the concentration of $B^{5+}-O-B^{5+}$ triplets with overbonded oxygens. In the $Ba(B_{1/3},B'_{2/3})O_3$ systems this energetic cost is not mitigated by short-range interactions so ordered phases are stable to high temperatures. In the $Pb-$systems however, the $Pb-O$ bonds to oxygens in $B^{2+}-O-B^{2+}$ triplets contract, and those towards $B^{5+}-O-B^{5+}$ triplets elongate (symmetry permitting). For example, in the $[110]_{NNM}$ supercell ($Pb(Mg_{1/3}Nb_{2/3})O_3$ stoichiometry) one third of the $Pb's$ are surrounded by 12 $B-O-B$ triplets only one of which is in configuration $Mg-O-Mg$, and the $Pb-O$ bond to the oxygen in this triplet is predicted to be only 2.38 $\AA$; bonds to oxygens in $B^{2+}-O-B^{5+}$ configurations are 2.63 $\AA$, and those in $B^{5+}-O-B^{5+}$ triplets are 2.86, 3.10, and 3.37$\AA$. The importance of hybridization between O $2p$ states and Pb $6s$ states in the ferroelectricity of $PbTiO_3$ was empahsized by Cohen(15) and Cohen and Krakauer (16); and by Bellaiche et al in discussing the ferroelectric properties of two $Pb(Zr_{1/3}Ti_{2/3})O_3$ supercells (18).

Qualitatively, the Bellaiche and Vanderbilt model appears to capture the essence of cation ordering in $Ba(B_{1/3},B'_{2/3})O_3$ systems, but it fails for the $Pb(B_{1/3},B'_{2/3})O_3$ systems, because it excludes short-range interactions; note that $[111]_{NNM}$ ($1:2$ ordering) is not the predicted GS for PZN or PMT (Figure 1). Bellaiche and Vanderbilt (14) suggested that covalency of short $Pb-O$ bonds might provide a mechanism for stabilizing $1:1$ order in place of $1:2$, but the specific mechanism was not explained. The essential point is not just that covalency of short $Pb-O$ bonds lowers the total energy, but that it **reduces the energies of electrostatically unfavorable configurations more than it reduces those of electrostatically favorable configurations.** In addition, the suggestion of Bellaiche and Vanderbilt that Pb^{4+} on $B-sites$ may be responsible for "the weak 1:1 order in PMN and PMT," fails to explain why, in the absence of octahedral Pb^{4+}, the range of $\Delta E's$ calculated for PMN and other $Pb(B_{1/3},B'_{2/3})O_3$ systems are so much smaller than those of the $Ba(B_{1/3},B'_{2/3})O_3$ systems. Evidently, $Pb(B_{1/3},B'_{2/3})O_3$ perovskites are more susceptible to disorder than their $Ba(B_{1/3},B'_{2/3})O_3$ counterparts because of the near cancellation of long- and short-range contributions to the excess configurational energy.

Attempts to fit a cluster expansion Hamiltonian (19) to the PMN results (Figure 2) indicate that more $\Delta E's$ are required to obtain a converged result; i.e a Hamiltonian that does not change significantly when one adds another effective cluster interaction. Absent a converged Hamiltonian with which to

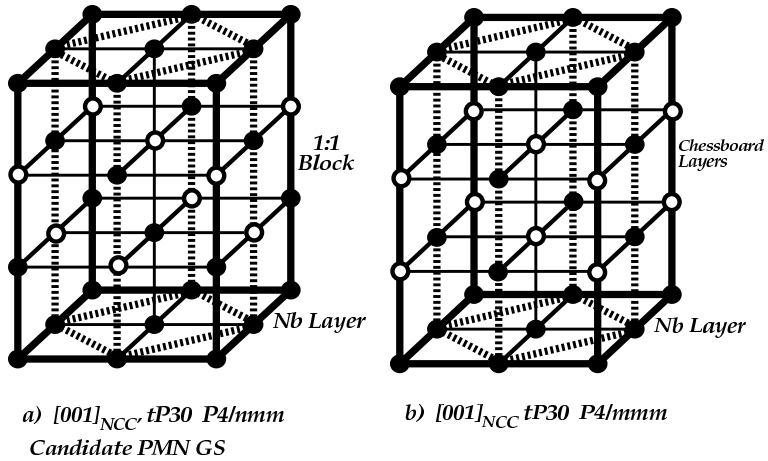

Fig. 4. a) The $[001]_{NCC'}$ structure a candidate PMN *Ground State*; b) the $[001]_{NCC}$ structure. Only $B-sites$ are shown, $\bullet = Nb$, $\circ = Mg$, dotted lines indicate unit cells. In both structures, $Nb-layers$ alternate with double chessboard layers, and in $[001]_{NCC'}$ the CC' layers can be regarded as $1:1-type$ blocks.

predict additional GS candidates, it is premature to claim a *prediction* that the $[001]_{NCC'}$ structure is the PMN GS.

3 Empirical Ising Model Calculations

Empirical Ising type models of cation ordering in $A(B_{1/3}, B'_{2/3})O_3$ perovskites(20), give substantial insight into the phase relations of PMN. Figures 5 and 6 are the phase diagrams one obtains from a simple three parameter model that was constrained to yield an absolute minimum energy at $X = 1/3$, and a $1:2 \rightarrow 1:1 \rightarrow DIS$ transition sequence: Figure 5 is part of the *mostly metastable* $PbNbO_3 - PbMgO_3$ pseudobinary, and Figure 6 shows order parameters for the $1:2$ and $1:1$ phases as functions of temperature. The first principles calculations suggest that $1:2$ is not the GS of PMN, but it is very close in energy to the leading candidate, $[001]_{NCC'}$. More to the point however, the specific GS structure has little or no effect on phase relations at temperatures of interest. Time fluctuations of the $1:2$ order parameter, $\eta_{1:2}$ (Figure 7), remain essentially zero, while of the $1:1$ order parameter, $\eta_{1:1}$ fluctuates dramatically. Fluctuations of $\eta_{1:1}$ correspond to the formation and dissolution of ordered microdomains. The large difference between $\eta_{1:2}$ and $\eta_{1:1}$ occurs because the stable $1:2 \rightleftharpoons 1:1$, and metastable $1:2 \rightleftharpoons DIS$, transitions are $first-order$, whereas the $1:1 \rightleftharpoons DIS$ transition is a line of *critical points*. In PMN the $1:1 \rightleftharpoons DIS$ phase boundary may or may not intersect the $X = 1/3$ composition (as it does in Figures 5 and 6) but it clearly does in PMT, where $1:1$ LRO is observed after 12 hours annealing at $T \leq 1350°C$(5). In *both* cases, the $1:1 \rightleftharpoons DIS$ transition passes sufficiently close to $X = 1/3$, that *equilibrium* $1:1$ SRO is stable

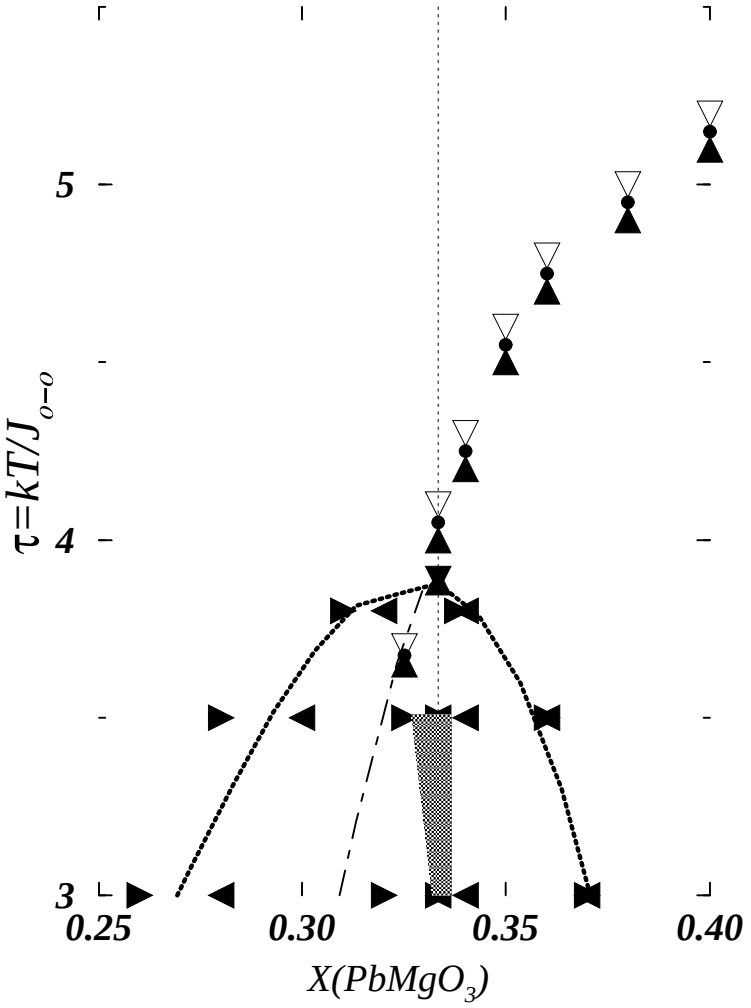
5
4
3
τ=kT/J_o-o
0.25
0.30
0.35
0.40
X(PbMgO_3)

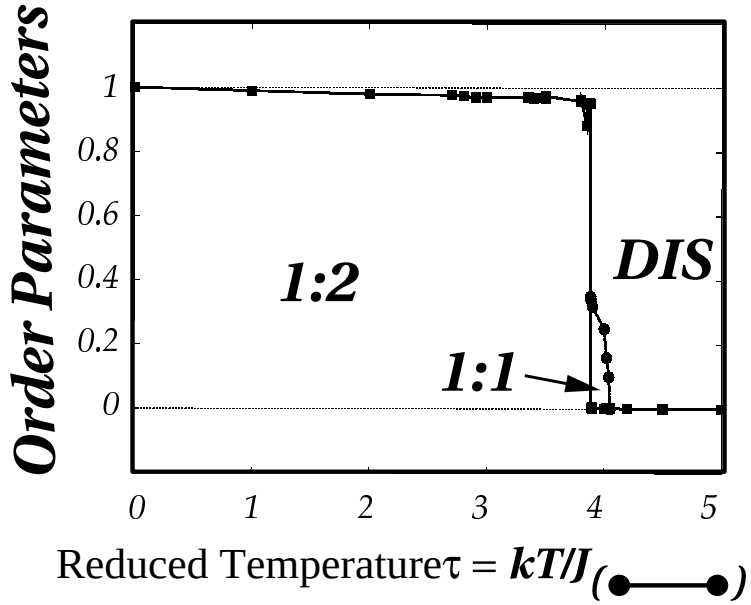

Fig. 6. Order parameters for the $1:2$ and $1:1$ phases as functions of temperature at the $X = 1/3$ composition.

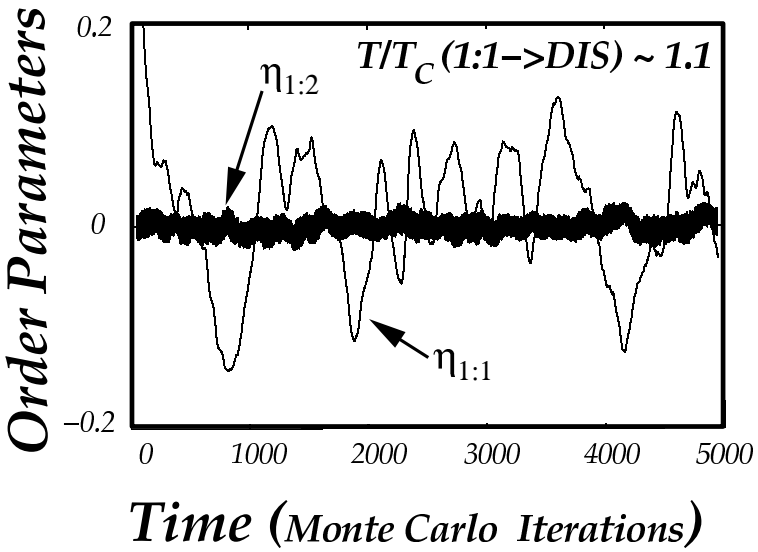

Fig. 7. Monte Carlo time fluctuations, at $T = 1.1T_c(1:1)$, of the order parameters $\eta_{1:2}$ *and* $\eta_{1:1}$, for the $1:2$ - and $1:1$ -phases respectively.

- In PMN, unfavorable kinetics prevent formation of either a $1:1$ intermediate temperature phase, or the GS. In PMT, the $1:1$ phase does form, the GS does not.
- The observed PMN microstructure is approximately the equilibrium state at the $(composition, temperature)$ point $(X = 1/3,\ T = T_B)$, where T_B is the blocking temperature for $B - site$ cation diffusion.
- Because the line of $1:1 \rightleftharpoons DIS$ transitions is a line of *critical points* the region above this transition is characterized by large fluctuations of $\eta_{1:1}$, as

shown in Figure 7.

- In PMT, the point $(X = 1/3,\ T = T_B)$ occurs *below* the $1:1 \rightleftharpoons DIS$ transition, so $1:1$ LRO is experimentally realized; i.e. domains grow.

The approximately equilibrium nature of SRO explains why ordered microregions in PMN do not coarsen even after prolonged annealing; there is no driving force for coarsening of equilibrium SRO. In PMT however, T_B occurs below $T_c(1:1)$, and therefore $1:1$ LRO is established after 12 hours annealing at $T \leq 1350°C$(5). Failure of $1:1$ ordered microdomains to coarsen is not evidence in support of the space-charge model, rather it is reflective of equilibrium state of SRO in PMN. A second problem with the space-charge model is that it requires a difference in bulk composition between ordered microregions and disordered matrix, but such a difference has not been observed (21). Note that fluctuations of $\eta_{1:1}$ can occur independent of charge, or compositional, fluctuations.

5 Conclusions

First principles total energy calculations suggest that the $[001]_{NCC'}$ structure may be the PMN GS. Although this is not a prediction of the GS per se, the $[001]_{NCC'}$ structure is a plausible candidate because of its similarity to the $1:1$ phase.

Comparing the first principles calculations for $Ba(B_{1/3}, B'_{2/3})O_3$ perovskites with those for their $Pb(B_{1/3}, B'_{2/3})O_3$ counterparts indicates that the long-range Coulomb interactions which drive $B-site$ ordering in the $Ba-$systems do not produce the same results in the Pb-systems. Apparently, hybridization between $O\ 2p$ states and $Pb\ 6s$ states stabilizes otherwise high energy configurations such as $B^{2+}-O-B^{2+}$ triplets, leading to a near cancellation of long- and short-range contributions to the configurational energy.

Empirical phase diagram calculations suggest a simple alternative to the space-charge model which is entirely consistent with experimental evidence. In particular, the failure of PMN ordered microdomains to coarsen is not evidence in support of the space-charge model, rather it indicates that the line of critical points that constitute the $1:1 \rightleftharpoons DIS$ transition is sufficiently close to T_B (blocking temperature for $B-site$ diffusion) to induce substantial *equilibrium* $1:1$ SRO.

6 Acknowledgements

The author gratefully acknowledges the assistance of G. Kresse with VASP calculations; M. Wensell with crystallographic problems and useful discussions; P.K. Davies with discussions of experimental data; and an anonymous referee for suggesting that I include more discussion of long-range interactions.

References

[1] H.B. Krause, J.M. Cowley and J. Wheatley, Acta. Cryst. **A35** 1015- (1979).
[2] J. Chen, H.M. Chan, and M. Harmer, J. Am Ceram. Soc. **72**[**4**], 593 (1989).
[3] T. Egami, W. Dmowski, S. Teslic, P.K. Davies, I.-W. Chen, and H. Chen, Ferroelectrics, 206-207, 231 (1998)
[4] C.A. Randall and A.S. Bhalla, Japn. J. Appl. Phys. 29(2), 327 (1990).
[5] M.A. Akbas and P.K. Davies J. Amer. Ceram. Soc. **80**(11), 2933 (1997).
[6] U. Treiber and S. Kemmler-Sack, J. Solid State Chem., **43**, 51- (1982).
[7] S. Kawashima, M. Nishida, I. Ueda, and H. Ouchi, J. Am. Ceram. Soc. **66**[**6**], 421, (1983).
[8] C-C. Lee, C-C Chou, and D-S. Tsai, Ferroelectrics 206, 293 (1998).
[9] E. Husson, M. Chubb and A. Morell, Mat. Res. Bull. **23** 357, (1988).
[10] H.D. Rosenfeld and T. Egami, Ferroelectrics **158**, 351 (1994)
[11] D. Viehland and J.-F. Li, J. Appl. Phys. **74**, 4121 (1993)
[12] N. de Mathan, E. Husson, G. Calvarin, J.R. Gavarri, A. Hewatt, and A. Morell, J. Phys.: Cond. Matter **3**, 8159 (1991)
[13] G. Kresse and J. Hafner, Phys. Rev. B **47**, 558 (1993); G. Kresse, Thesis, Technische Universität Wien 1993; Phys. Rev. B **49**, 14 251 (1994). G. Kresse and J. Furthmüller, Comput. Mat. Sci. **6**, 15 (1996); Phys. Rev. **54**, 11169 (1996). See also http://tph.tuwien.ac.at/ vasp/guide/vasp.html for further details.
[14] L. Bellaiche and D. Vanderbilt, PRL **81**, 1318 (1998).
[15] R. E. Cohen Nature **358**, 136 (1992).
[16] R. E. Cohen and H. Krakauer, Ferroelectrics **136**, 65 (1992).
[17] L. F. Mattheiss, Phys. Rev. **B6**, 4718 (1972).
[18] L. Bellaiche, J. Padilla and D. Vanderbilt, First Principles Calculations for Ferroelectrics, R.E. Cohen Ed. AIP, CP **436**, 11- (1998).
[19] J.M. Sanchez, F. Ducastelle, and D. Gratias, Physica **128A**, 334 (1984).
[20] B.P. Burton, Phys. Rev. **B59**, 1 (1999).
[21] Viehland paper this volume.